JACS
JOURNAL OF THE AMERICAN CHEMICAL SOCIETY

Article

pubs.acs.org/JACS

Ditopic Ambiphilicity of an Anionic Dimetalloborylene Complex

Holger Braunschweig,* Alexander Damme, Rian D. Dewhurst, Thomas Kramer, Sebastian Östreicher, Krzysztof Radacki, and Alfredo Vargas

Institut für Anorganische Chemie, Julius-Maximilians-Universität Würzburg, Am Hubland, 97074 Würzburg, Germany

Supporting Information

ABSTRACT: In early reports, the boron atom of the anionic borido complexes $[\{(\eta^5\text{-}C_5H_4R)(OC)_2Mn\}_2B]^-$ (R = H, Me) showed nucleophilic behavior in the presence of electrophiles such as methyl iodide and group 11 metal chlorides, akin to the ground-breaking boryl lithium of Yamashita and Nozaki. Later, a reaction with the well-known transition metal Lewis base $[Pt(PCy_3)_2]$ suggested the possibility of boron-centered electrophilicity. In this paper we elucidate a third reactivity profile of the anion, nucleophilic substitution on heavier halides of group 14 metals by a manganese center. Meanwhile, other group 11 halides were found to interact with the boron center, but form structures different from those seen with gold. The basis of the discrimination of the anion between main group and transition metal halides is explored computationally, and the ditopic, ambiphilic reactivity of the anions is discussed.

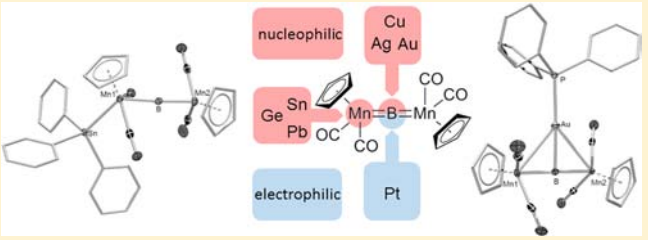

INTRODUCTION

The preparation of boryl anions has been a challenge for chemists for nearly 60 years now, and the prospect of a boron-centered nucleophilic species[1] that is isoelectronic to a carbene[2] has attracted great interest. This is due to the impact of organoboron species on organic and organometallic synthesis[3] and their growing importance as molecular materials and sensors.[4] Conventional protocols of organoboron synthesis such as hydroboration[5] or silicon−boron exchange[6] are restricted to the use of inherently electrophilic boranes. Thus, boryl anions offer the unique opportunity to introduce nucleophilic boron centers, thereby vastly extending the range of possible transformations. However, attempts to obtain such compounds through the reduction of boron−halide bonds have until recently been hindered by the very reactive boryl radical that is formed as an intermediate, which almost instantly undergoes side reactions such as dimerization[7] or hydrogen abstraction[7b] from solvent molecules.

Since the synthesis of the first (mono)boryl anion (**1**) in 2006 through reduction of a bromodiazaborole by the group of Nozaki and Yamashita,[8] boryl anions have been a small and slowly, yet steadily, growing class of compounds (Chart 1). The availability of **1** is made possible by the sterically demanding Dip (Dip = 2,6-bis(diisopropyl)phenyl) substituents at the nitrogen atoms, which prevent dimerization of the presumed radical intermediate, and the electronic stabilization of the boryl center by the adjacent nitrogen atoms. Contributions by other groups to the synthesis of novel boryl anions include the NHC-stabilized borole **3** that was reported four years later by our research group[9] and the similarly NHC-stabilized boryl anion **4** that could not be isolated but is considered as a feasible intermediate in the reduction of the corresponding iodoborane and trapping reactions with several electrophiles.[10] The anionic compound **2b** was generated in 2008 by our group by reduction of $[\{(\eta^5\text{-}C_5H_4Me)(OC)_2Mn\}_2BCl]$ and stands out from the other anions due to its *sp*-hybridized boron atom and consequently linear geometry.[11] For this reason, we classified it as an anionic metalloborylene rather than a boryl anion. One of the most interesting features of these compounds is their reactivity. All of them show, to different extents, nucleophilic behavior at the boron center. Complex **1** has been reported to react with a variety of carbon electrophiles[12] as well as transition metal chlorides,[13] rare-earth metal complexes,[14] and even boranes[15] and alanes.[16]

Formally (boron-centered) nucleophilic reactions of **2** with methyliodide[11] and [ITolAuCl][17] were reported previously, leading to $[\{(\eta^5\text{-}C_5H_4Me)(OC)_2Mn\}_2BMe]$ and trimetalloborido complex **7** (see Scheme 2). In addition, the somewhat discordant addition of Lewis basic fragment $[Pt(PCy_3)]$ to the boron atom led to a Lewis adduct complex.[18] These results suggest an ambiphilic character of the boron atom, which despite its apparent nucleophilic character is able to receive a dative bond from a metal base.[9] While **3** was reported to add Me^+ (from MeI) and H^+ (from $[Et_3NH]Cl$) to the nucleophilic boron center, **4** undergoes a great variety of reactions with carbon electrophiles.[10]

Herein, we present reactivity studies of **2** toward p- and d-block metals, revealing a highly unusual ditopicity at the already ambiphilic molecule.

RESULTS AND DISCUSSION

Synthetic, Structural, and Spectroscopic Results. Since treatment of **2** with alkyl halides other than methyl iodide gave poor results, the scope of reactants was extended to

Received: November 5, 2012
Published: January 18, 2013

   dx.doi.org/10.1021/ja310895w | *J. Am. Chem. Soc.* 2013, 135, 2313−2320

Chart 1. Currently Known Boron-Centered Nucleophiles

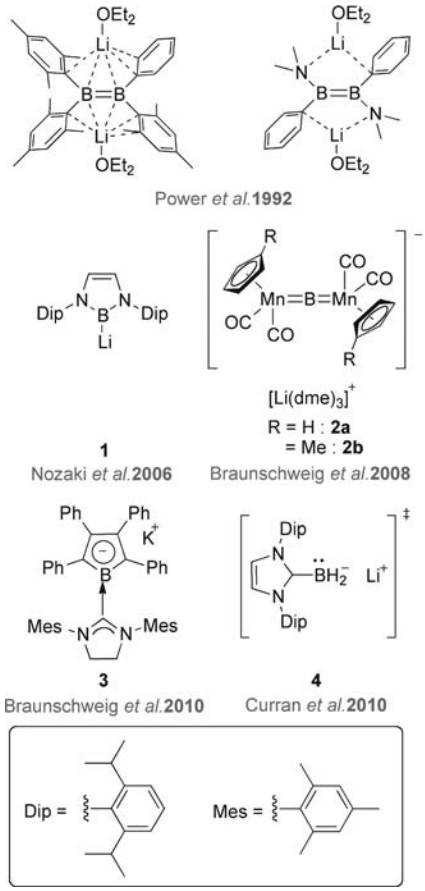

electrophiles of heavier group 14 elements. When a solution of **2a** was treated with an equimolar amount of Me_3GeCl, a color change to bright yellow and an upfield shift of the ^{11}B NMR signal from 195 ppm to 179 ppm was observed. The ^{1}H NMR spectrum indicated an unsymmetrically substituted molecule. Repeating the reaction with Me_3SnCl produced almost identical results: the reaction mixture turned bright yellow, and a ^{11}B NMR signal at 179 ppm was observed along with a splitting of the Cp ^{1}H NMR signal. Unfortunately, the structures of the products could not be clarified conclusively. However, reacting bulkier Ph_3SnCl with **2a** proved more successful in elucidating the molecular structure of these products. After the color change and high-field shift of the ^{11}B NMR signal (σ = 177 ppm) were observed, the reaction mixture was concentrated and stored at −32 °C for several days. Yellow needle-shaped crystals suitable for X-ray structure determination were obtained from this solution. Single crystal X-ray crystallography showed the formation of a product (**5**) resulting from a reaction at one of the manganese atoms of **2a** (Figure 1).

The Sn−Mn1 distance (263.69(5) pm) of **5** is shorter than the sum of the covalent radii of manganese and tin (280.1 pm) and within the range of Mn−Sn distances found in other triaryltin compounds of manganese. Unlike in **2**, the B−Mn bonds in **5** are not of the same length. The bond to the Mn-atom carrying the Ph_3Sn ligand (194.2(4) pm) is significantly elongated with respect to the Mn2−B distance (182.6(4) pm), indicating a notable weakening of the bond by coordination of Sn to Mn1. A similar bond weakening was monitored in $[\{(\eta^5\text{-}C_5H_4Me)(OC)_2Mn\}_2B(AuITol)]$, which can be prepared from **2b** and [ITolAuCl][17] as a result of an interaction of the Au-

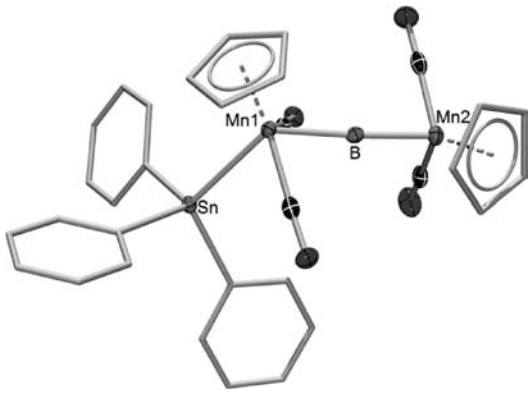

Figure 1. Molecular structure of **5**. Thermal ellipsoids represent 50% probability. Ellipsoids of the Cp ligands and the Ph groups, as well as all hydrogen atoms, are omitted for clarity. Selected bond lengths [pm] and angles [deg]: Sn−Mn1 263.96(5), Mn1−B 194.2(4), Mn2−B 182.6(4); Sn−Mn1−B 126.78(11), Mn1−B−Mn2 176.9(2).

atom with one of the Mn-atoms. On the other hand, the Mn1−B−Mn2 angle of **2a** does not seem to be affected by the coordination of $SnPh_3$ and remains almost linear in **5** (176.9(2)°). ^{1}H and ^{13}C NMR spectra of **5** again show a splitting of the respective Cp-associated resonance into two signals (^{1}H: σ = 4.99, 4.69 ppm; ^{13}C: σ = 85.5, 82.6 ppm), fitting well with the unsymmetrical molecular structure.

Following the same pattern as in the other reactions with electrophiles of heavier group 14 elements, **6**, a lead analogue of **5**, was prepared from **2a** and Ph_3PbCl. Again, a high-field shift of the ^{11}B NMR signal (σ = 177 ppm) and the two ^{1}H signals of the inequivalent Cp ligands (σ = 4.46 and 4.39 ppm) were observed. Yellow cubic crystals were obtained by concentrating the reaction mixture after filtration at −32 °C, confirming the existence of **6** (Figure 2).

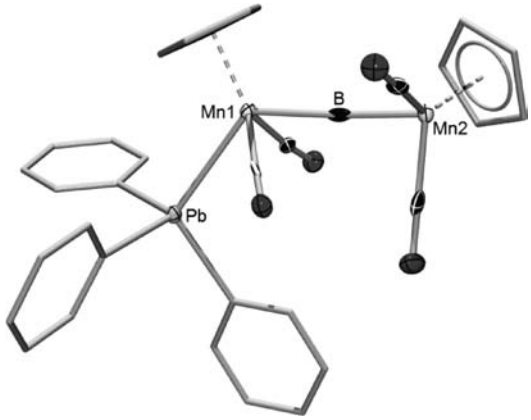

Figure 2. Molecular structure of **6**. Thermal ellipsoids represent 50% probability. Ellipsoids of the Cp ligands and the Ph groups as well as all hydrogen atoms are omitted for clarity. Selected bond lengths [pm] and angles [deg]: Pb−Mn1 270.27(7), Mn1−B 194.0(6), Mn2−B 181.1(6); Pb−Mn1−B 12.02(14), Mn1−B−Mn2 176.9(3).

The molecular structures of **6** and **5** are very similar. The Pb−Mn1 bond (270.27(7) pm) is shorter than the sum of the covalent radii of Mn and Pb (285 pm) and only slightly longer than the Sn−Mn1 bond in **5**. The Mn1−Pb bond (194.0(6) pm) is elongated due to the coordination of the $PbPh_3$ ligand as seen in **5** while the Mn1−B−Mn2 angle is still almost linear (176.9(3)°).

dx.doi.org/10.1021/ja310895w | J. Am. Chem. Soc. 2013, 135, 2313−2320

Given the great similarities in the NMR spectral data such as the similar shift of the ^{11}B NMR signal and the splitting of the ^{1}H NMR signal of the Cp ligands observed in the reactions discussed above, it can be assumed that the reactions of Me_3GeCl and Me_3SnCl also take place at one of the Mn-atoms (Scheme 1).

Scheme 1. Reactions at the Mn Center of 2a

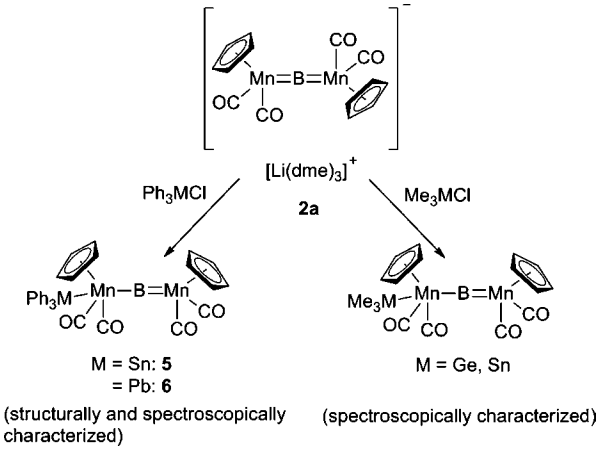

Reactions like these are well-known for anionic metallates of manganese[19] but are somewhat surprising in this case, given that **2** has until now only shown reactivity at the boron center.[11,17] The ability of the manganese atoms to act as formal nucleophiles is a clear experimental indication at the location of the negative charge in **2**, which was previously predicted to be at the manganese atoms rather than at the boron atom in computational investigations.[17]

In contrast, the reaction of **2b** with [ITolAuCl] was reported to take place at the boron center, leading to [{(η^5-C_5H_4Me)-$(OC)_2Mn$}$_2$B(AuITol)] (**7**) as mentioned above.[17] Complex **7** can be considered as a trimetalloboride complex and displays an interesting interaction of the Au-atom with one of the Mn-atoms. A classical bond between Au and Mn like the M–Mn bonds in **6** (M = Sn) and **7** (M = Pb) seems rather unlikely considering QTAIM analysis, which shows no bond critical point between Au and Mn, and a Wiberg bond index of only 0.16. Instead, NBO-results pointed toward a delocalized situation within the B–Au–Mn triangle. The picture of a relatively weak Au–Mn interaction is also underpinned by NMR spectroscopic data: in the ^{1}H and ^{13}C NMR spectra of **7** only one set of signals was observed for the methylcyclopentadiene (Cp′) ligands at the Mn-atoms (^{1}H: σ = 4.38, 4.26, 1.74 ppm; ^{13}C: σ = 82.7, 81.6, 14.3 ppm) at room temperature as well as at −90 °C, suggesting that the interaction between Au and Mn is readily broken in solution.

In order to extend this reactivity paradigm to other group 11 transition metal chlorides, a solution of **2a** in toluene was treated with [ITolAgCl] and stirred for 12 h at room temperature. A color change to dark orange and a deep-field shift of the ^{11}B NMR signal (σ = 212 ppm) was observed, indicating the formation of a trimetalloboride similar to **7**. Yellow crystals suitable for X-ray crystallographic analysis were obtained from the reaction mixture after filtration by slow evaporation of the solvent. The molecular structure confirms the formation of [{(η^5-C_5H_4Me)$(OC)_2Mn$}$_2$B(AgITol)] (**8**) (Figure 3), which in general shows great similarity to **7**. The B–Ag bond (218.1(13) pm) of **8** and B–Au bond (218.1(13) pm) of **7** are almost identical in length and the interaction between Ag and Mn is also present in **8**, best seen in the shortening of the bond from B to the affected Mn that was also noted in **7** (also in **5** and **6**). Nevertheless, the longer Mn2–Ag distance (279.3(3) pm) compared to to 265.1(4) pm for B–Au pm in **7** and the more linear B–Ag–$C_{Carbene}$ angle (167.3(5)°) account for an even weaker interaction than that found in **7**. In agreement with this, no splitting of the Cp signals was found in the ^{1}H or ^{13}C spectra of **8** (^{1}H: σ = 4.28 ppm; ^{13}C: σ = 81.0 ppm).

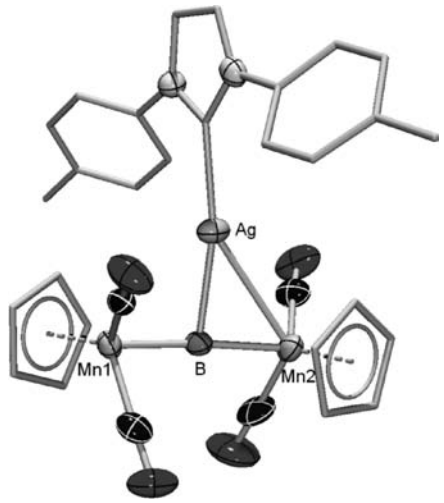

Figure 3. Molecular structure of **8**. Thermal ellipsoids represent 50% probability. Ellipsoids of the Cp and NHC ligands, and all hydrogen atoms, are omitted for clarity. Selected bond lengths [pm] and angles [deg]: B–Ag 218.1(13), B–Mn1 185.2(14), B–Mn2 193.9(14), Ag–Mn2 279.3(3); Mn1–B–Mn2 176.2(8), B–Ag–$C_{carbene}$ 167.3(5), Mn2–Ag–$C_{carbene}$ 148.9(3), Ag–B–Mn2 85.1(5).

The reaction of **2b** with [ITolCuCl] completes the row of group 11 transition metals. A mixture of the two compounds in toluene was stirred for 12 h until a single ^{11}B NMR signal at σ = 216 ppm was observed, and the solvent was slowly evaporated after filtration. After 2 days at −32 °C, orange crystals were obtained and the formation of [{(η^5-C_5H_4Me)$(OC)_2Mn$}$_2$B-(CuITol)] (**9**) was confirmed by X-ray crystallography (Figure 4).

In contrast to those of **7** and **8**, the Mn1–B (189.9(2) pm) and Mn2–B (189.1(2) pm) bond lengths are almost identical in **9**, indicating a weak influence of the Cu-atom. Likewise, the B–Cu–$C_{carbene}$ angle is almost linear (175.28(8)°) with only very minimal bending of the Cu toward Mn2. Looking at the B–M–$C_{carbene}$ (M = Au, Ag, Cu) angle in compounds **7** (153.0 (1)°), **8** (167.3(5)°), and **9** (175.28(8)°) gives a good picture of a M–Mn interaction that becomes weaker when going from Au to Cu. Unsurprisingly, the ^{1}H and ^{13}C NMR spectra of **9** show only one signal for the Cp ligands (^{1}H: σ = 4.31 ppm; ^{13}C: σ = 81.8 ppm) in compliance with the almost symmetric structure and the very weak Cu–Mn interaction that is readily broken in solution. As in the case of the trimetalloborides discussed above, a very low-field-shifted ^{11}B NMR signal (σ = 216 ppm) indicates the presence of three metal atoms in the coordination sphere of boron. This shift accounts for further deshielding at the boron atom by a transfer of electron density from the Mn_2B– to the MITol$^+$ fragment. A significant charge transfer between the Mn_2B^- and the AuITol$^+$ fragment has been confirmed for **7** in NPA-analysis.

dx.doi.org/10.1021/ja310895w | J. Am. Chem. Soc. 2013, 135, 2313−2320

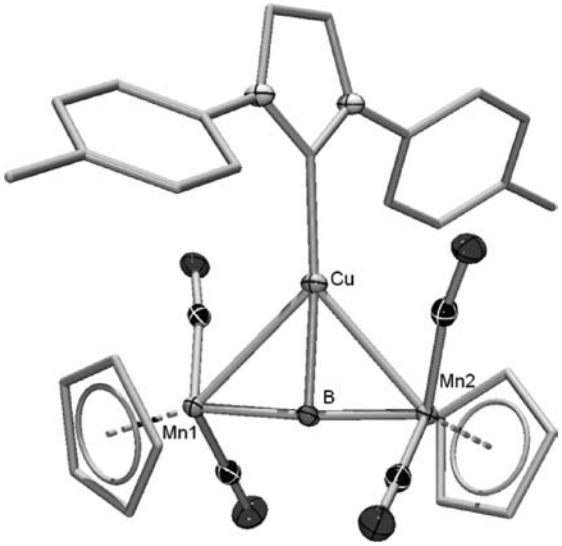

Figure 4. Molecular structure of **9**. Thermal ellipsoids represent 50% probability. Ellipsoids of the Cp and NHC ligands, and all hydrogen atoms, are omitted for clarity. Selected bond lengths [pm] and angles [deg]: B–Cu 197.97(18), B–Mn1 189.1(2), B–Mn2 189.9(2), Cu–Mn1 265.29(6), Cu–Mn2 271.86(6); Mn1–B–Mn2 174.9(11), B–Cu–$C_{carbene}$ 175.28(8).

The influence of the substituent at the group 11 metal atom became apparent when the reaction was repeated with [(Ph_3P)AuCl]: a solution of **2b** and [(Ph_3P)AuCl] in toluene was stirred for 8 h until a color change to bright orange and the typical low-field shift of the ^{11}B NMR signal could be observed. The reaction mixture was then filtered and stored at −32 °C to obtain orange crystals suitable for X-ray crystallographic analysis. As expected, the formation of the trimetalloboride **10** was confirmed.

The molecular structure of **10** (Figure 5) is surprisingly similar to that of **9**. In contrast to **7** or **8**, a weak interaction

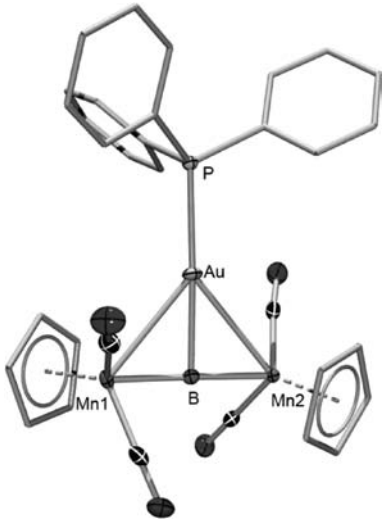

Figure 5. Molecular structure of **10**. Thermal ellipsoids represent 50% probability. Ellipsoids of the Cp and Ph groups, and all hydrogen atoms, are omitted for clarity. Selected bond lengths [pm] and angles [deg]: B–Au 211.2(3), B–Mn1 190.2(3), B–Mn2 190.9(3), Au–Mn1 285.09(4), Au–Mn2 287.03(4); Mn1–B–Mn2 178.2(2), B–Au–P 172.30(9).

from Au to both Mn-atoms is observed, indicated by a nearly linear B–Au–P angle (172.30(9)°) and B–Mn bonds (190.2(3) and 190.9(3) pm) of almost identical length. As a possible reason for this difference, the electronic influence of the relatively electron-poor PPh_3 ligand, resulting in an overall lower electron density at the Au atom, can be contemplated.

Together with the previously reported reaction of **2a** with [$Pt(PCy_3)_2$],[18] which results in the formation of the T-shaped Lewis base adduct **11**, the boron atom of **2** can therefore be considered as an ambiphilic reactive center. An overview of the reactivity at that center is given in Scheme 2.

Scheme 2. Reactions at the Boron Center of 2

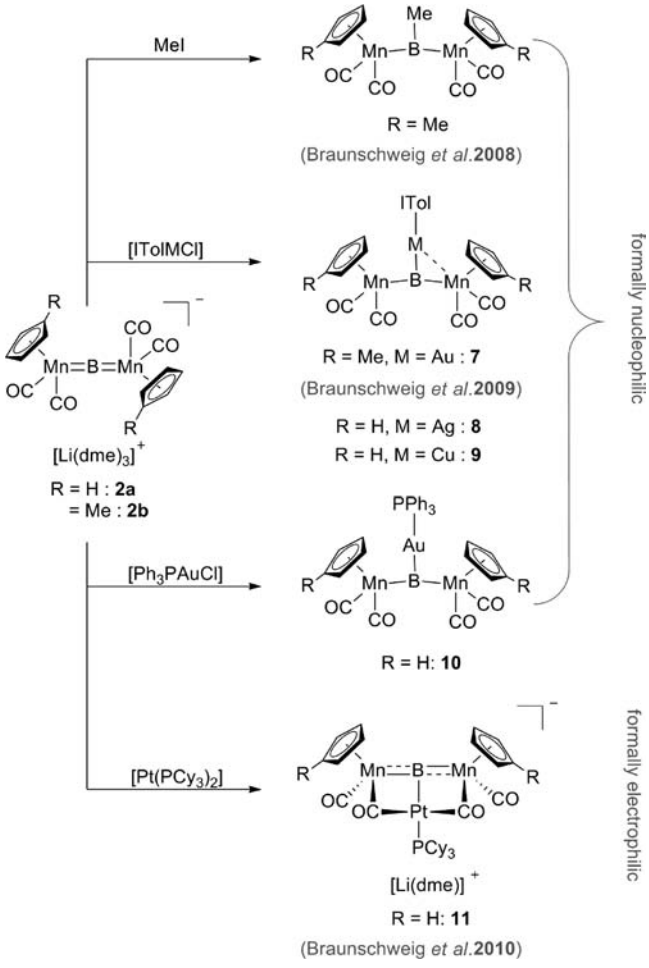

With MeI, [ITolMCl] (M = Au, Ag, Cu), and [Ph_3PAuCl], **2** undergoes formally nucleophilic substitution reactions that have also been reported for **1**. The formation of the Lewis base stabilized metalloboride **11** with [$Pt(PCy_3)_2$], on the other hand, demonstrates the electrophilic nature of **2** that until now has only been observed in neutral metalloborides.

Quantum-Chemical Calculations. We sought to reveal the physicochemical reasons as to why the LCu^+ moiety preferably binds at the boron atom of the [{(η^5-C_5H_5)-$(OC)_2Mn$}$_2$B]$^-$ (hereafter referred to as [MnBMn]$^-$) unit whereas Ph_3Sn^+ instead binds to one of the Mn-centers.[20] We set out to determine which energetic factors govern the stability of **5** and **9**, as the two extremes of the addition to **2a**; i.e., **5** bears a Ph_3Sn group bound solely to Mn, and **9**, a [Cu(ITol)] fragment bound equidistant to both Mn-centers. The special

dx.doi.org/10.1021/ja310895w | J. Am. Chem. Soc. 2013, 135, 2313−2320

behavior of the $[\{(\eta^5\text{-}C_5H_4Me)(OC)_2Mn\}_2B]^-$ anion was also scrutinized by way of comparison to the structurally related and isoelectronic $[\{(\eta^5\text{-}C_5H_4Me)(OC)_2Fe\}_2B]^+$ cation[21] and the neutral $[(\eta^5\text{-}C_5H_5)(OC)_2Mn{=}B{-}Fe(CO)_2(\eta^5\text{-}C_5Me_5)]$ complex[22] designated hereafter as [M−B−M]. Kohn−Sham Density Functional Theory (DFT) calculations were undertaken for **5** and **9**, energy minimizations were carried out at the B3LYP/Def2-SVP[23,24] level, and bonding analysis was conducted within B3LYP/TZP[25−29] on the optimized structures. Optimization and Natural Bonding Orbital (NBO)[30,31] analysis of the [M−B−M] complexes were carried out at the B3LYP/6-311+G*[23,32−38] level.

The Energy Decomposition Analysis (EDA), also known as the "fragment approach",[39−42] as implemented in the Amsterdam Density Functional (ADF) program was employed for the description of the bonding situation. Using EDA, the interaction energy E_{int} associated with the interaction between the fragments (LCu^+ or Ph_3Sn^+) and $[MnBMn]^-$ can be divided into three components: $E_{int} = E_{elstat} + E_{Pauli} + E_{orb}$. The first term, E_{elstat}, corresponds to the classical electrostatic interaction between the unperturbed charge distributions of the fragments (the overall density being the superposition of the fragment densities). The second term, E_{Pauli}, expresses the energy change that arises upon going from the simple superposition of the fragment densities to the wave function that obeys the Pauli principle through antisymmetrization and normalization of the product of the fragment wave functions. In the last term, E_{orb}, the energy that originates from the contributions from stabilizing orbital interactions (electron pair bonding, charge transfer, polarization) is given. Table 1 provides the values of the different bonding energy components for **5** and **9**.

Table 1. Interaction Energy (kcal/mol) Components in LCu-[MnBMn] and L_3Sn-[MnBMn] Systems

	5	9
E_{elstat}	−159.67	−164.17
E_{orb}	−117.77	−81.89
E_{Pauli}	129.40	121.98
E_{int}	−148.04	−124.08

The electrostatic interaction in **9** is greater than the orbital interaction; i.e., it constitutes ∼70% of the total E_{elstat} and E_{orb} energies, whereas in **5** this value amounts to ∼60%. It is evident that the $[MnBMn]^-$ anion binds more strongly to Ph_3Sn^+ than to LCu^+, the orbital interaction being a larger part in the former. It should be recalled that the orbital interaction energy is stabilizing because the destabilizing interactions originating from the two-orbital four-electron interactions have been taken into account in the Pauli interactions. Close examination suggests that the interactions are instead closed-shell interactions under the polarization effect of the boron atom, itself gaining charge with concomitant charge depletion at the Mn-centers.

In both cases, the frontier orbitals of $[MnBMn]^-$ are unusually high on the energy scale with respect to those of the LCu^+ or Ph_3Sn^+ units, which makes the five highest energy orbitals of **9** consist mainly of those of the $[MnBMn]^-$ fragment; thus the frontier orbitals of the complex are mainly centered on the Mn-atoms. In contrast, the frontier orbitals of $[MnBMn]^-$ interact with the frontier orbitals of Ph_3Sn^+ to form the HOMO−3 and energetically lower MOs in **5**, while those of LCu^+ begin to interact only with the HOMO−4 of the $[MnBMn]^-$ fragment (Figure 6). This is in line with the more

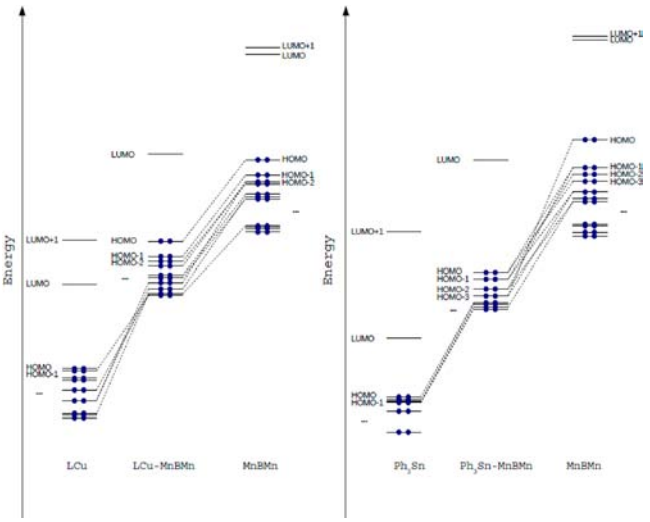

Figure 6. Major orbital−orbital interactions between the LCu and Ph_3Sn fragments and the MnBMn fragment. Not all interactions are shown, and only major contributions are depicted.

pronounced orbital interactions observed between the anion and the p-block metal. In **9**, there is no apparent electron delocalization between the Cu- and B-atoms, at least in terms of frontier orbitals; instead the HOMO reveals that the Cu interacts to a small extent with the Mn-atoms, suggesting a predominantly electrostatic nature of the interaction (see Figure 7). On the other hand, the presence of Ph_3Sn^+ disrupts

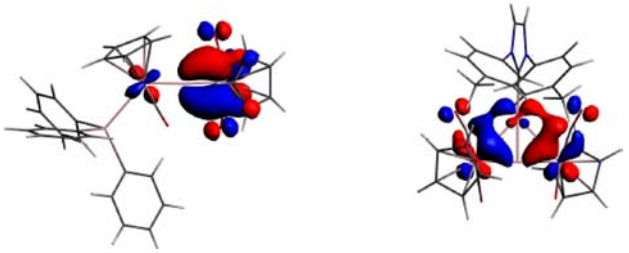

Figure 7. HOMO−1 of **5** (left) and HOMO of **9** (right).

the orbital symmetry of the $[MnBMn]^-$ anion, which produces a remarkable polarization of the Mn−Mn segment (Mulliken charge: −0.38 versus −0.94), suggesting an induced and highly tunable reactivity of the Mn-centers (see Figure 7). Moreover, there are clear bonding MOs centered on the Sn−Mn bond which is a clear sign of covalent interaction between the two moieties.

Natural Population Analysis within the NBO formalism was carried out. Figure 8 shows the calculated natural charge and natural population of the complexes $[\{(\eta^5\text{-}C_5H_4Me)(OC)_2Fe\}_2B]^+$, $[\{(\eta^5\text{-}C_5H_4Me)(OC)_2Mn\}_2B]^-$, and $[(\eta^5\text{-}C_5H_5)(OC)_2Mn{=}B{-}Fe(CO)_2(\eta^5\text{-}C_5Me_5)]$. The electrostatic potential of each complex is additionally mapped on a plane containing the M−B−M unit with red depicting a negative charge and blue indicating a positive charge. It is evident that in all three cases—the cation, the neutral compound, and the anion—the boron atom bears a positive charge while the metals are negatively charged. In the case of $[\{(\eta^5\text{-}C_5H_4Me)$-

dx.doi.org/10.1021/ja310895w | J. Am. Chem. Soc. 2013, 135, 2313−2320

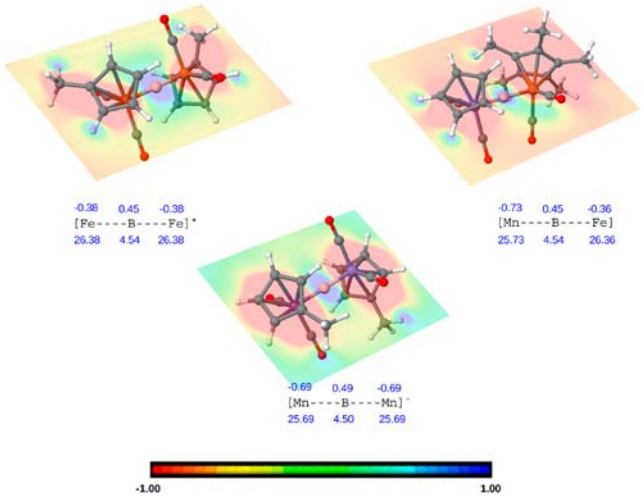

Figure 8. Molecular electrostatic potential (MEP), natural charge, and natural population in three [M−B−M] complexes.

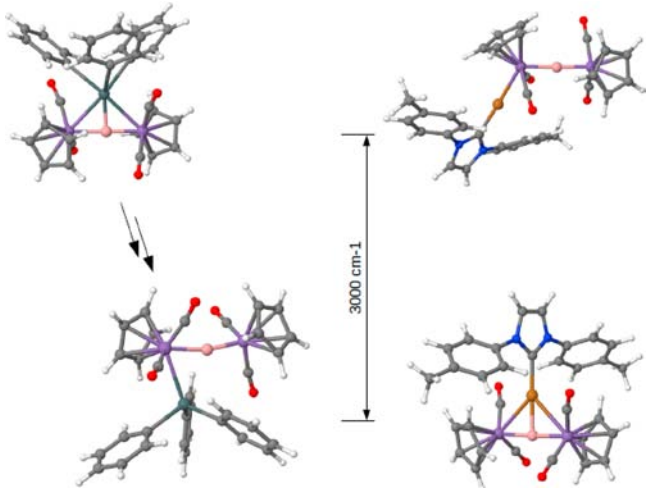

Figure 9. "Inversed" geometries of Ph_3Sn-[MnBMn] and LCu-[MnBMn].

$(OC)_2Mn\}_2B]^-$, being anionic, the excess negative charge is clearly more centered on the Mn-atoms, whose natural charge amounts to −0.69, compared to the iron atoms in the $[\{(\eta^5\text{-}C_5H_4Me)(OC)_2Fe\}_2B]^+$ cation. Despite these differences, the natural charge at boron is almost constant (0.45−0.49) over the three complexes. It is interesting to note that it is not the anionic complex in which the Mn carries the most negative charge but rather the neutral [MnBFe] system (−0.73 versus −0.69). In the unsymmetrical [MnBFe] complex, *both* the boron and the iron atoms are depleted of charge and concomitantly allow charge build-up on the manganese atom. In other words, the Mn-atom can strip the charge not only from the adjacent boron but also from the iron, even if this atom is not directly bound to it. Such a mechanism can be observed in a symmetrical complex provided that one of the Mn-atoms interacts with a cation as demonstrated in the case of **5** (see above). This illustrates the formidable ability of boron to act as a charge flux bridge when intercalated between two charge-labile metals. This property probably owes its existence to the presence of the empty p_z orbital of boron, which permits diverse forms of bonding to both of the metal centers.

Upon optimization starting from the inversed geometry (i.e., the Ph_3Sn and LCu positions are interchanged), calculations show that the Ph_3Sn moiety finds itself attached to only one of the Mn-atoms whereas the LCu^+ fragment can remain bound to one Mn but at an accompanying energetic cost (see Figure 9). Results from the Ph_3Sn^+ fragment calculations reveal that the frontier orbitals of this fragment are mainly centered on the aryl rings and it is only from the HOMO−5 that a p orbital is available for bonding, which, as shown above in the orbital diagram, is already too low in energy (and does not have the correct symmetry) to favorably interact with the Mn-atoms. In the case of LCu^+, although it is the HOMO−4 that interacts with the $[MnBMn]^-$ fragment to form the HOMO of the trinuclear complex (see Figure 7), the Cu d_{yz} orbital component interacts with the Mn-atoms.

In order to test the possibility of steric control of the addition to either boron or manganese in these systems, energy minimization calculations on the $[\{(\eta^5\text{-}C_5H_5)(OC)_2Mn\}_2B]^-$ fragment with either the $SnMe_3$ or $SnPh_3$ group bound at the boron atom were performed. In both cases, no minimum was found and the stannyl group migrated to a Mn-center, in line with experimental observations. Geometry optimizations in which Cu(ITol) and smaller Cu(IMe) groups were bound to a Mn-center did provide enegery minima; however in both cases these were ca. 9 kcal/mol less stable than the centrally bound isomers. Both sets of calculations suggest that the size of the substituent has little bearing on its ultimate point of attachment.

We conclude that the discrimination demonstrated by the ditopic base between the d and p block metals could be ascribed to (a) the induced reactivity of the Mn atoms, which preferably bind covalently to p-block metals for reasons of orbital energy and symmetry, or (b) if these cannot be fulfilled, then the electrophile attacks at boron where it can favorably interact electrostatically and orbitally with the Mn centers as well as the boron atom. Another interesting feature of the $[MnBMn]^-$ anion is its high reactivity due to its high-lying frontier orbitals that can nevertheless readily react with species having frontier orbitals that are (much) lower in energy, this facility being aided by the boron atom's versatile ability to mediate the redirection of charge flux.

■ CONCLUSION

The reactivity of the anionic metalloboride **2** has been studied intensively. Reactions with [ITolAgCl] and [ITolCuCl] have produced the trimetalloborides **8** and **9** similar to the already known trimetalloboride **7**. From the molecular structures of **7**, **8**, and **9**, a trend for the interesting M−Mn interaction that was first observed in **7** can be deduced. The interaction becomes undoubtedly weaker when going from Au to Cu as the central metal, indicated by the $B-M-C_{carbene}$ angle, which is significantly bent in **7** but effectively linear in **9**. Likewise, exchanging the NHC ligand at the group 11 metal with a phosphine significantly weakens the M−Mn interaction, which is clearly visible in the almost linear B−Au−P angle of **10**, prepared from **2a** and $[Ph_3PAuCl]$.

Meanwhile, reactions of **2a** with halides of Ge, Sn, and Pb have unveiled a second reactive center of **2**. Molecular structures of **5** and **6** confirm a reaction at one of the Mn atoms instead of the boron atom. This leaves the overall impression of an anionic metalloboride with two reactive centers, one of which shows electrophilic tendencies when reacted with $[Pt(PCy_3)_2]$.

dx.doi.org/10.1021/ja310895w | J. Am. Chem. Soc. 2013, 135, 2313−2320

■ ASSOCIATED CONTENT

Supporting Information

Experimental and crystallographic details. This material is available free of charge via the Internet at http://pubs.acs.org.

■ AUTHOR INFORMATION

Corresponding Author

h.braunschweig@uni-wuerzburg.de

Notes

The authors declare no competing financial interest.

■ ACKNOWLEDGMENTS

Financial support from the European Research Council (Advanced Investigator Grant to H.B.) is gratefully acknowledged.

■ REFERENCES

(1) Wagner, M.; Hommes, N. J. R. V.; Nöth, H.; Schleyer, P. v. R. *Inorg. Chem.* **1995**, *34*, 607−614.

(2) (a) Kirmse, W. *Carbene Chemistry*, 2nd ed.; Academic Press: New York, 1971. (b) Wentrup, C. *Reactive Molecules*; Wiley: New York, 1984. (c) Moss, R. A.; Jones, M., Jr. *Carbenes*, Vol. I; Wiley: New York, 1973. (d) Moss, R. A.; Jones, M., Jr. *Carbenes*, Vol. II; Wiley: New York, 1975. (e) Dekker, M. *Carbene Chemistry*; New York, 2005. (f) Bourissou, D.; Guerret, O.; Gabbaï, F. P.; Bertrand, G. *Chem. Rev.* **2000**, *100*, 39−91.

(3) (a) Irvine, G. J.; Lesley, M. J. G.; Marder, T. B.; Norman, N. C.; Rice, C. R.; Robins, E. G.; Roper, W. R.; Whittell, G. R.; Wright, L. J. *Chem. Rev.* **1998**, *98*, 2685−2722. (b) Marder, T. B.; Norman, N. C. *Top. Catal.* **1998**, *5*, 63−73. (c) Mkhalid, I. A. I.; Barnard, J. H.; Marder, T. B.; Murphy, J. M.; Hartwig, J. F. *Chem. Rev.* **2010**, *110*, 890−931. (d) Hartwig, J. F. *Acc. Chem. Res.* **2012**, *45*, 864−873. (e) Braunschweig, H.; Dewhurst, R. D.; Schneider, A. *Chem. Rev.* **2010**, *110*, 3924−3957.

(4) (a) Entwistle, C. D.; Marder, T. B. *Angew. Chem., Int. Ed.* **2002**, *41*, 2927−2931. (b) Entwistle, C. D.; Marder, T. B. *Chem. Mater.* **2004**, *16*, 4574−4585. (c) Braunschweig, H.; Rais, D. *Angew. Chem., Int. Ed.* **2005**, *44*, 7826−7828. (d) Jaekle, F. *J. Inorg. Organomet. P.* **2005**, *15*, 293−307. (e) Hudson, Z. M.; Wang, S. N. *Dalton Trans.* **2011**, *40*, 7805−7816. (e) Hudson, Z. M.; Wang, S. N. *Acc. Chem. Res.* **2009**, *42*, 1584−1596. (f) Cheng, F.; Jaekle, F. *Polym. Chem.* **2011**, *10*, 2122−2132.

(5) (a) Mannig, D.; Nöth, H. *Angew. Chem., Int. Ed. Engl.* **1985**, *24*, 878−879. (b) Burgess, K.; Ohlmeyer, M. J. *Chem. Rev.* **1991**, *91*, 1179−1191. (c) Wadepohl, H. *Angew. Chem., Int. Ed. Engl.* **1997**, *36*, 2441−2444. (d) Beletskaya, I.; Pelter, A. *Tetrahedron* **1997**, *53*, 4957−5026. (e) Ishiyama, T.; Miyaura, N. *J. Organomet. Chem.* **2000**, *611*, 392−402. (f) Crudden, C. M.; Edwards, D. *Eur. J. Org. Chem.* **2003**, 4695−4712.

(6) (a) Cui, C. Z.; Bonder, E. M.; Qin, Y.; Jakle, F. *J. Polym. Sci., Part A: Polym. Chem.* **2010**, *48*, 2438−2445. (b) Chen, P.; Jäkle, F. *J. Am. Chem. Soc.* **2011**, *133*, 20142−20145. (c) Chen, P.; Lalancette, R. A.; Jäkle, F. *J. Am. Chem. Soc.* **2011**, *133*, 8802−8805. (d) Kuhtz, H.; Cheng, F.; Schwedler, S.; Böhling, L.; Brockhinke, A.; Weber, L.; Parab, K.; Jäkle, F. *ACS Macro Lett.* **2012**, *1*, 555−559. (e) Qin, Y.; Shipman, P. O.; Jakle, F. *Macromol. Rapid Commun.* **2012**, *33*, 562−567.

(7) (a) Brotherton, R. J. *Progress In Boron Cemistry*, Vol. 1; Pergamon: New York, 1964. (b) Weber, L.; Schnieder, M.; Lonnecke, P. *J. Chem. Soc., Dalton Trans.* **2001**, 3459−3464. (c) Marder, T. B. *Product Subclass 3: Diborane(4) Compounds*; Science of Synthesis; Georg Thieme Verlag: Stuttgart-New York, 2005; Vol. *6*.

(8) (a) Segawa, Y.; Yamashita, M.; Nozaki, K. *Science* **2006**, *314*, 113−115. (b) Braunschweig, H. *Angew. Chem., Int. Ed.* **2007**, *46* (12), 1946−1948.

(9) Bauer, J.; Braunschweig, H.; Dewhurst, R. D. *Chem. Rev.* **2012**, *112*, 4329−4346.

(10) (a) Braunschweig, H.; Chiu, C. W.; Radacki, K.; Kupfer, T. *Angew. Chem., Int. Ed.* **2010**, *49*, 2041−2044. (b) Braunschweig, H.; Chiu, C.-W.; Kupfer, T.; Radacki, K. *Inorg. Chem.* **2011**, *50*, 4247−4249. (c) Monot, J.; Solovyev, A.; Bonin-Dubarle, H.; Derat, E.; Curran, D. P.; Robert, M.; Fensterbank, L.; Malacria, M.; Lacote, E. *Angew. Chem., Int. Ed.* **2010**, *49*, 9166−9169.

(11) Braunschweig, H.; Burzler, M.; Dewhurst, R. D.; Radacki, K. *Angew. Chem., Int. Ed.* **2008**, *47*, 5650−5653.

(12) Segawa, Y.; Suzuki, Y.; Yamashita, M.; Nozaki, K. *J. Am. Chem. Soc.* **2008**, *130*, 16069−16079.

(13) Segawa, Y.; Yamashita, M.; Nozaki, K. *Angew. Chem., Int. Ed.* **2007**, *46*, 6710−6713.

(14) Li, S. H.; Cheng, J. H.; Chen, Y. H.; Nishiura, M.; Hou, Z. M. *Angew. Chem., Int. Ed.* **2011**, *50*, 6360−6363.

(15) Hayashi, Y.; Segawa, Y.; Yamashita, M.; Nozaki, K. *Chem. Commun.* **2011**, *47*, 5888−5890.

(16) Dettenrieder, N.; Dietrich, H. M.; Schadle, C.; Maichle-Mossmer, C.; Tornroos, K. W.; Anwander, R. *Angew. Chem., Int. Ed.* **2012**, *51*, 4461−4465.

(17) Braunschweig, H.; Brenner, P.; Dewhurst, R. D.; Kaupp, M.; Müller, R.; Ostreicher, S. *Angew. Chem., Int. Ed.* **2009**, *48*, 9735−9738.

(18) Braunschweig, H.; Kraft, K.; Ostreicher, S.; Radacki, K.; Seeler, F. *Chem.—Eur. J.* **2010**, *16*, 10635−10637.

(19) Duffy, D. N.; Nicholson, B. K. *J. Organomet. Chem.* **1979**, *164*, 227−234.

(20) Both the Gaussian03 (http://www.gaussian.com/) and ADF (http://www.scm.com) suites of programmes were used for the calculations. Spin restricted calculations were performed by constraining the projection of the total electronic spin along a reference axis to zero. The zeroth-order regular approximation (ZORA) was employed for complexes containing 4d and 5d metals. Frequency calculations were conducted to determine if each stationary point corresponds to a minimum. The Jmol program (http://www.jmol.org/) and the Graphical User Interface (ADF-GUI, a part of the ADF package) were used for vizualisation purposes.

(21) Braunschweig, H.; Kraft, K.; Kupfer, T.; Radacki, K.; Seeler, F. *Angew. Chem., Int. Ed.* **2008**, *47*, 4931.

(22) Bauer, J.; Braunschweig, H.; Dewhurst, R. D.; Kraft, K.; Radacki, K. *Chem.—Eur. J.* **2012**, *18*, 2327.

(23) Becke, A. D. *J. Chem. Phys.* **1993**, *98*, 1372.

(24) Weigend, F.; Ahlrichs, R. *Phys. Chem. Chem. Phys.* **2005**, *7*, 3297.

(25) Stephens, P. J.; Devlin, F. J.; Chabalowski, C. F.; Frisch, M. J. *J. Phys. Chem.* **1994**, *98*, 11623.

(26) Chong, D. P. *Mol. Phys.* **2005**, *103*, 749.

(27) Chong, D. P.; van Lenthe, E.; van Gisbergen, S. J. A.; Baerends, E. J. *J. Comput. Chem.* **2004**, *25*, 1030.

(28) van Lenthe, E.; Baerends, E. J. *J. Comput. Chem.* **2003**, *24*, 1142.

(29) Raffenetti, R. C. *J. Chem. Phys.* **1973**, *59*, 5936.

(30) Weinhold, F.; Landis, C. R. *Valency and Bonding: A Natural Bond Orbital Donor-Acceptor Perspective*; Cambridge University Press: Cambridge, U.K., 2005.

(31) Reed, A. E.; Curtiss, L. A.; Weinhold, F. *Chem. Rev.* **1988**, *88*, 899.

(32) McLean, A. D.; Chandler, G. S. *J. Chem. Phys.* **1980**, *72*, 5639.

(33) Krishnan, R.; Binkley, J. S.; Seeger, R.; Pople, J. A. *J. Chem. Phys.* **1980**, *72*, 650.

(34) Wachters, A. J. H. *J. Chem. Phys.* **1970**, *52*, 1033.

(35) Hay, P. J. *J. Chem. Phys.* **1977**, *66*, 4377.

(36) Raghavachari, K.; Trucks, G. W. *J. Chem. Phys.* **1989**, *91*, 1062.

(37) Clark, T.; Chandrasekhar, J.; Spitznagel, G. W.; Schleyer, P. v. R. *J. Comput. Chem.* **1983**, *4*, 294.

(38) Frisch, M. J.; Pople, J. A.; Binkley, J. S. *J. Chem. Phys.* **1984**, *80*, 3265.

(39) Bickelhaupt, F. M.; Baerends, E. J. Kohn-Sham Density Functional Theory: Predicting and Understanding Chemistry. In *Reviews in Computational Chemistry*; Lipkowitz, K. B., Boyd, D. B., Eds.; Wiley-VCH: New York, 2000.

(40) te Velde, G.; Bickelhaupt, F. M.; Baerends, E. J.; Fonseca Guerra, C.; van Gisbergen, S. J. A.; Snijders, J. G.; Ziegler, T. *J. Comput. Chem.* **2001**, *22*, 931.
(41) Morokuma, K. *Acc. Chem. Res.* **1977**, *10*, 294.
(42) Ziegler, T.; Rauk, A.; Baerends, E. J. *Theor. Chim. Acta* **1977**, *43*, 261.